JOC The Journal of Organic Chemistry

ARTICLE

pubs.acs.org/joc

Computational Study on the Mechanism and Selectivity of C−H Bond Activation and Dehydrogenative Functionalization in the Synthesis of Rhazinilam

Corey S. Ellis and Daniel H. Ess*

Department of Chemistry and Biochemistry, Brigham Young University, Provo, Utah 84602, United States

Supporting Information

ABSTRACT: The key platinum mediated C−H bond activation and functionalization steps in the synthesis of (−)-rhazinilam (Johnson, J. A.; Li, N.; Sames, D. *J. Am. Chem. Soc.* **2002**, *124*, 6900) were investigated using the M06 and B3LYP density functional approximation methods. This computational study reveals that ethyl group dehydrogenation begins with activation of a primary C−H bond in preference to a secondary C−H bond in an insertion/methane elimination pathway. The C−H activation step is found to be reversible while the methane elimination (reductive elimination) transition state controls rate and diastereoselectivity. The chiral oxazolinyl ligand induces ethyl group selectivity through stabilizing weak interactions between its phenyl group (or cyclohexyl group) and the carboxylate group. After C−H activation and methane elimination steps, Pt−C bond functionalization occurs through β-hydride elimination to give the alkene platinum hydride complex.

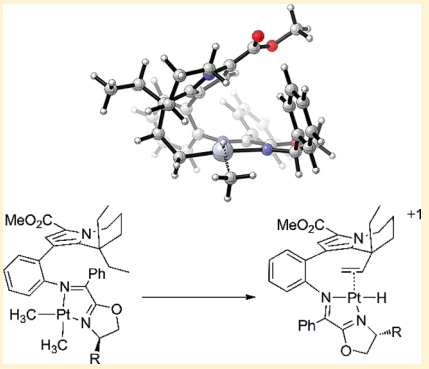

1. INTRODUCTION AND BACKGROUND

Direct, selective activation and functionalization of C−H bonds offers an attractive strategy for concise construction of complex synthetic targets.[1] This often involves a transition metal complex that coordinates and activates a C−H bond to give a metal alkyl or aryl species that is then functionalized (Scheme 1a).[2−4] High chemoselectivity, regioselectivity, and reactivity can be achieved by the use of a directing group, such as an imine, that brings the transition metal center into close proximity of the C−H bond to promote coordination and cleavage (Scheme 1b).[5] This strategy has recently been employed in the synthesis of (+)-lithospermic acid,[6] (−)-incarvillateine,[7] and (−)-rhazinilam.[8−11]

The asymmetric synthesis of the antitumor alkaloid rhazinilam using C−H activation reported by Sames and co-workers is intriguing because it results in the functionalization of an unactivated sp^3 C−H bond.[8] The reported synthetic route is briefly outlined in Scheme 2.[8] Pyrrole annulation followed by installation of a methyl carboxylate group gave compound **1** that was then reacted with 2-benzoylpryidine and dimethyl platinum $[Me_2Pt(\mu\text{-}SMe_2)]_2$ to give the chiral oxazolinyl chelated dimethyl platinum complex **2**. Addition of 1 equiv of triflic acid resulted in protonation of the platinum dimethyl species to liberate 1 equiv of methane and a mixture of diastereomers **3a** and **3b** in a nonequivalent ratio. Subsequent thermolysis at temperatures between 60 and 70 °C resulted in C−H activation and dehydrogenative functionalization to give platinum hydrides **7a** and **7b**. Treatment with aqueous KCN and then hydroxyl amine gave **8a** and **8b**. After isolation of **8a**, this diastereomer was converted to (−)-rhazinilam (**9**) in two steps that involved carbonylation, macrolactamization, and ester deprotection.

Scheme 1. (a) Outline of C−H Bond Activation and Functionalization Strategy; (b) Generalization of Imine Directed C−H Bond Activation

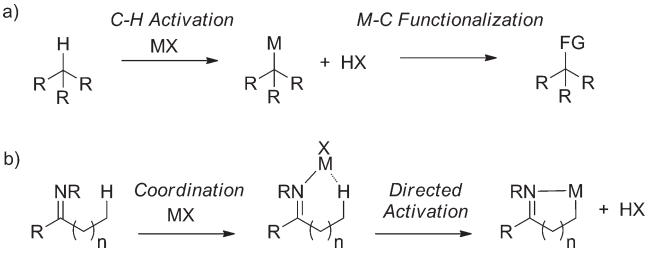

The best diastereoselectivity reported was obtained at 60 °C and gave a 6:1 ratio of **7a** to **7b** for the phenyl oxazolinyl ligand and a 7.5:1 ratio of **7a** to **7b** for the cyclohexyl oxazolinyl ligand (Scheme 2). At 70 °C the selectivity was reduced to a 3:1 and 4.4:1 ratio for the phenyl and cyclohexyl oxazolinyl ligands, respectively. Importantly, Sames and co-workers reported that during 72 h of reaction time the ratio of **3a** to **3b** remained constant. In addition, the ratio of **8a** to **8b** also remained constant but different than the **3a** to **3b** ratio. This result suggests that during thermolysis **3a** and **3b** equilibrate as **7a** and **7b** are formed and that the diastereoselectivity is the result of competing reaction pathways.

Because there are relatively few reactions that both activate and functionalize unactivated sp^3 C−H bonds we have used

Received: June 13, 2011
Published: August 04, 2011

Scheme 2. Reported Asymmetric Synthesis of (−)-Rhazinilam (see ref 8)

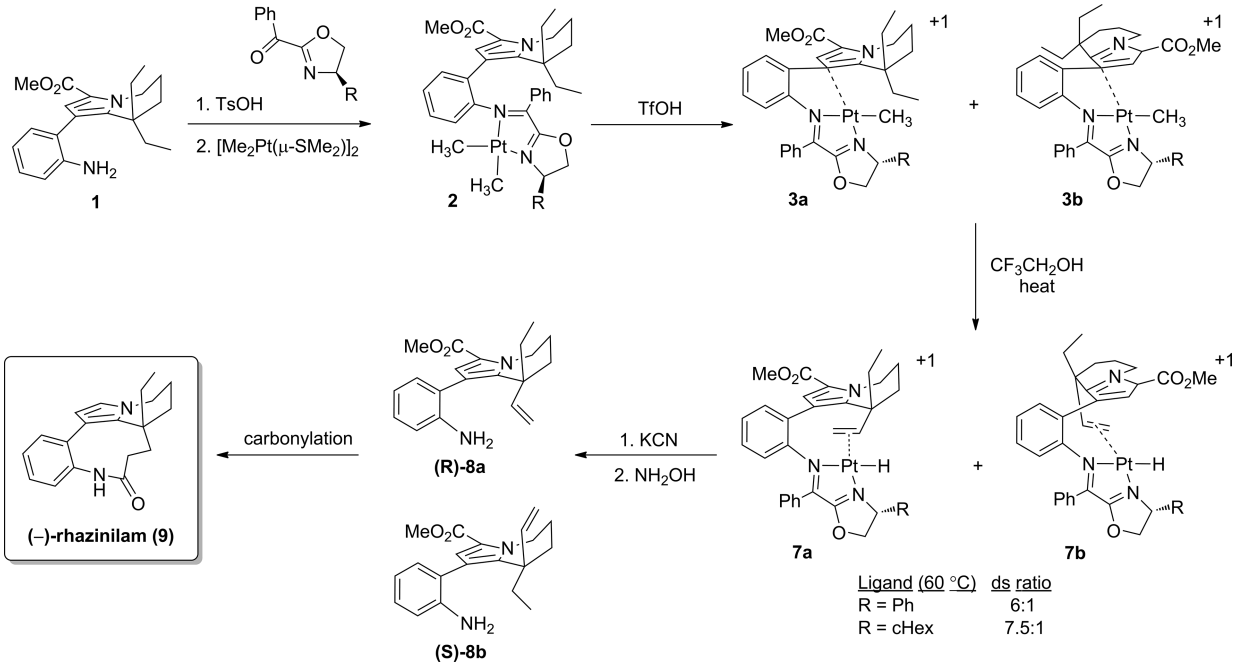

density functional theory to unravel the mechanism and stereoselectivity in the conversion of the methyl platinum complexes **3a,b** into the platinum hydrides **7a,b**. In doing this we have answered several questions that may be germane to the general class of chelate assisted C−H activation reactions used in synthesis. (1) How important and what is the nature of C−H bond coordination prior to activation? (2) Is there a regioselective preference for activation/cleavage of the methylene or terminal ethyl group C−H bond? (3) Is the C−H bond broken via an insertion (oxidative addition) or metathesis pathway? (4) What transition state(s) controls the rate and/or diastereoselectivity? (5) How does the chiral oxazolinyl group control preference for ethyl group dehydrogenative functionalization?

2. COMPUTATIONAL METHODS

All stationary points were confirmed as minima or first-order saddle points by full calculation of the Hessian. Only the lowest energy minima or transition state is reported. Several different structures differing in ethyl group orientation and ring conformation were explored. M06[12]/6-31G(d,p)[LANL2DZ] optimizations were carried out in Gaussian 09 with an ultrafine integration grid.[13,14] B3LYP[15] optimizations were carried out in Gaussian 03.[16] 3D ball and stick structures were rendered using CYLview.[17] The M06 method, a hybrid meta functional, was designed for broad applicability including transition metals, main group thermochemistry, and medium-range correlation energy.[18] Several recent computational benchmark and experimental comparative studies show that M06 is the most accurate functional currently available for organometallic systems.[19] Unless otherwise noted all reported energy values are free energies in the gas phase at 298 K. For some of the key stationary points we also evaluated the M06 electronic energies with the larger 6-311+G(2d,p)/LAN2TZ(f)[20] (triple ζ LAN2TZ basis set augmented with a single f polarization exponent of 0.993 for Pt) basis set. In addition, we also computed solvation free energies (ΔG_{solv}) relative to the gas phase for 2,2,2-trifluoroethanol with the IEFPCM-SDM[21] solvent model using the 6-31G(d,p)[LANL2DZ] basis set. The larger basis set and free energy of solvation corrected energies are explicitly noted in the text.

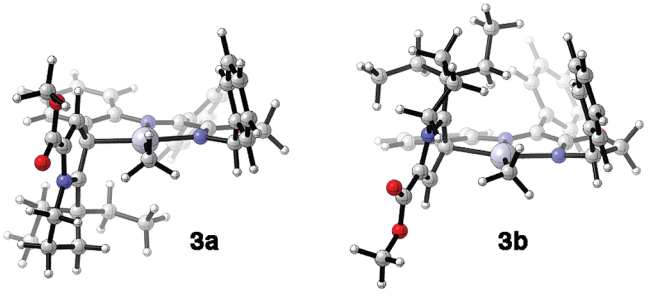

Figure 1. M06 optimized η-1 coordination complexes.

3. RESULTS AND DISCUSSION

3.1. C−H Bond Coordination. The diastereomers **3a** and **3b** that are generated upon protonation of complex **2** (R = Ph, Scheme 2) have an η-1 coordination between the C-4 carbon of the pyrrole ring and the platinum metal center (Figure 1). M06 geometries and energetics show that for complex **3a** coordination between the Pt center and the C-4 carbon of the pyrrole ring is more stable than coordination to the C-3 carbon by 5.9 kcal/mol of free energy and 1.9 kcal/mol in enthalpy. Relative to **3a**, M06 predicts diastereomer **3b** to be only 0.1 kcal/mol higher in free energy. Interestingly, **3b** is predicted to be −1.4 kcal/mol lower in enthalpy relative to diastereomer **3a**. Similarly, B3LYP optimized geometries and energies predict **3a** to be lower in free energy than **3b** by 0.8 kcal/mol but 0.4 kcal/mol higher in enthalpy. **3a** is more stable than **3b** due to entropy effects.

C−H activation of **3a** begins when the pyrrole ligand dissociates to create a vacant coordination site on Pt to allow for C−H bond coordination. Several agostic complexes were found

dx.doi.org/10.1021/jo201234f |J. Org. Chem. 2011, 76, 7180–7185

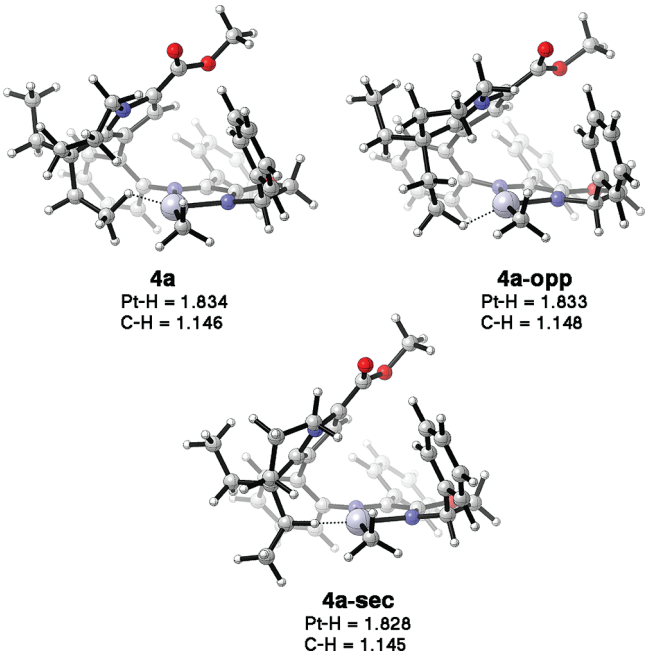

Figure 2. C−H bond coordination complexes.

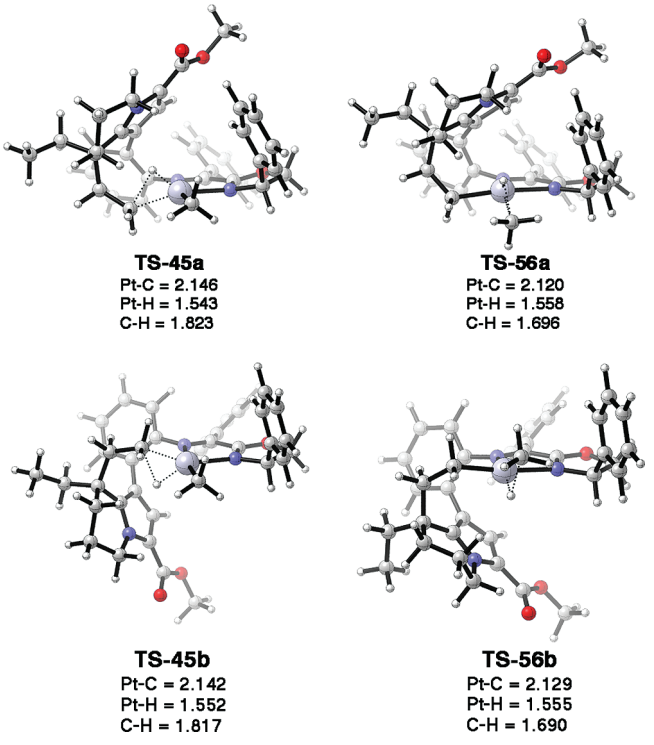

Figure 3. Insertion (oxidative addition) and methane elimination transition states.

for coordination of one of the ethyl group C−H bonds. The most favorable agostic C−H interaction occurs with the primary C−H bond in structure **4a** (Figure 2). The combination of pyrrole ligand dissociation and C−H bond coordination gives **4a** that is endergonic by 14.0 kcal/mol relative to **3a**. Surprisingly, coordination of the methyl C−H bond in the opposite direction (**4a-opp**) requires 19.4 kcal/mol. Coordination of the methylene

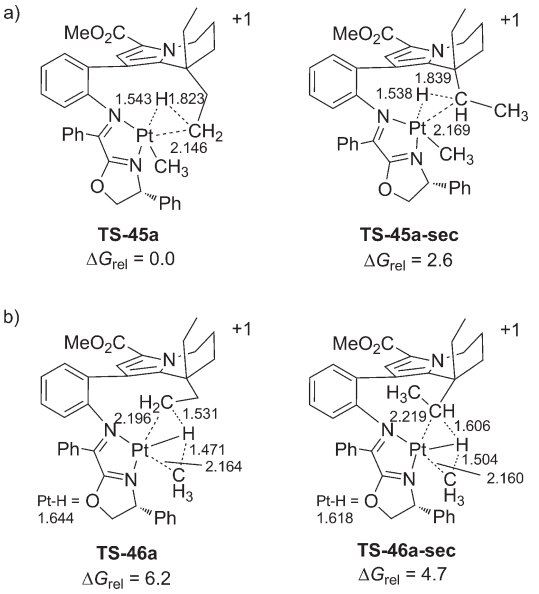

Figure 4. Lowest energy (a) insertion and (b) metathesis C−H cleavage transition states.

C−H bond in **4a-sec** is 1.0 kcal/mol higher in free energy than **4a** (ΔG = 15.0 kcal/mol). The coordinated C−H bonds in **4a** and **4a-sec** can be considered to have genuine agostic interactions. The Pt−H distance in **4a** is 1.834 Å and in **4a-sec** is 1.828 Å. The C−H bond distances increase from 1.099 Å in **3a** to 1.146 Å and 1.145 Å in **4a** and **4a-sec**, respectively.

3.2. C−H Cleavage Transition States. From the C−H bond coordination complexes we explored several possible C−H bond insertion (oxidative addition) and σ-bond metathesis pathways. As expected, the lowest energy transition state for C−H bond cleavage occurs via an insertion transition state **TS-45a** (Figures 3 and 4, $\Delta G^{\ddagger}$ = 27.0 kcal/mol; $\Delta H^{\ddagger}$ = 24.0 kcal/mol).[22] However, there is a 2.6 kcal/mol free energy and 4.1 kcal/mol enthalpy preference for insertion into the stronger primary C−H bond via **TS-45a** than activation of a weaker methylene C−H bond (**TS-45a-sec**, Figure 4). This result is in contrast to the proposal by Sames and co-workers of initial C−H bond activation at the methylene carbon.[8b] **TS-45a** gives the platinum hydride intermediate with the hydride on the same side as the pyrrole and oxazolinyl phenyl group (**5a**; see Figure 5 in Section 3.3). The insertion transition state to give the alternative platinum hydride intermediate, which corresponds to complex **4a-opp**, is several kcal/mol higher in enthalpy and free energy than **TS-45a**. In **TS-45a** the C−H bond is elongated to 1.823 Å and the Pt−H and Pt−C bonds are nearly fully formed at 1.543 and 2.146 Å. Inspection of this insertion transition state geometry reveals that the origin for activation of the stronger C−H bond is the result of developing ring strain. Insertion into the primary C−H bond leads to a nine-member metallacycle that is more favorable than the eight-member metallacycle. This energy difference also shows up as an ∼5 kcal/mol thermodynamic preference of the corresponding platinum hydride intermediate.

On the free energy surface the metathesis transition states, **TS-46a** and **TS-46a-sec** (Figure 4), are 6.2 and 4.7 kcal/mol higher in energy than **TS-45a**. On the enthalpy surface these transition states are both 5.3 kcal/mol higher in energy than **TS-45a**.[23] In the metathesis transition states the rupturing C−H bond lengths are significantly shorter than the partial C−H bond lengths in the

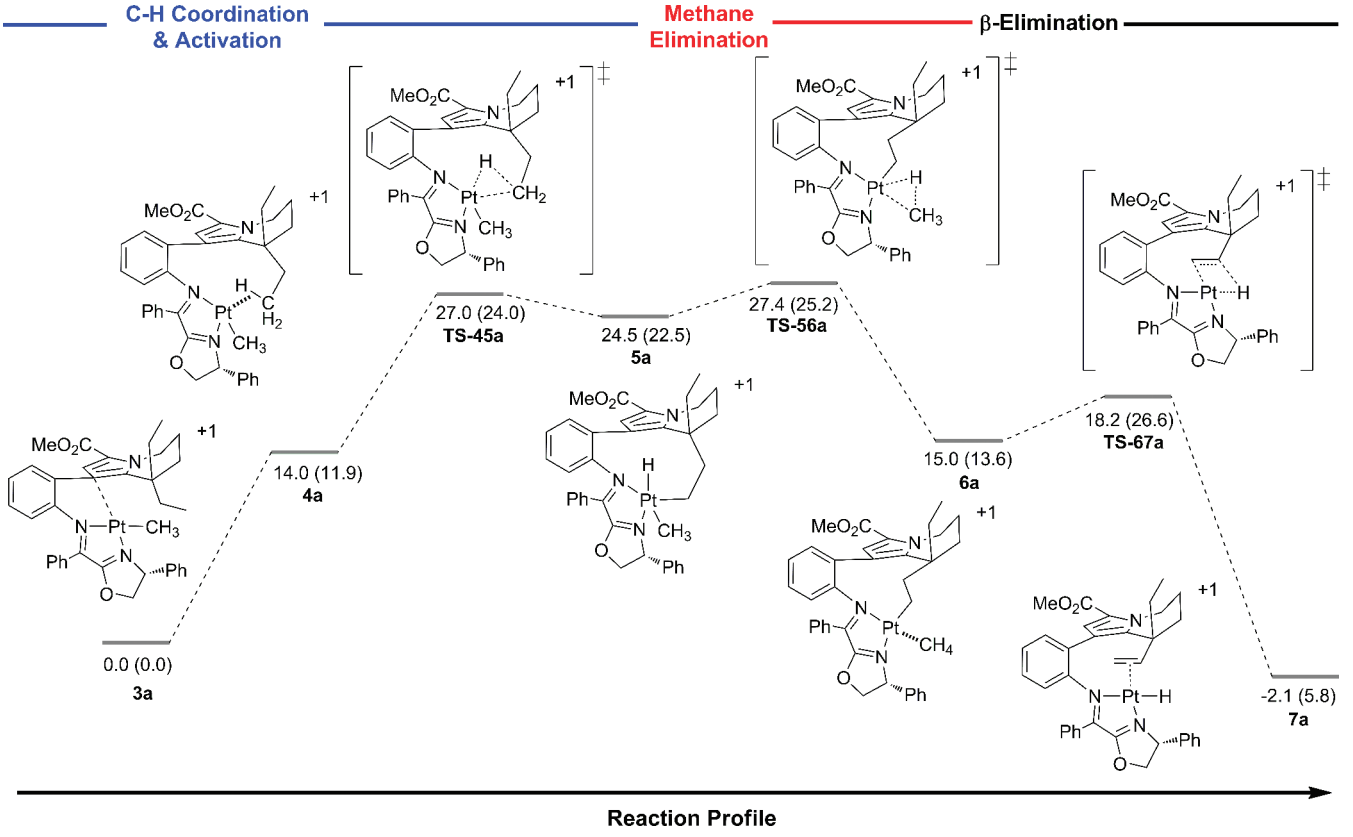

Figure 5. M06 free energy (enthalpy) at 298 K profile. The methane dissociation intermediate preceding **TS-67a** is not shown.

insertion transition states. In addition, these transition states have significant Pt-hydride character and lead directly to the methane complex **6a** (see Figure 5 in Section 3.3).

3.3. Complete Energy Surface. C−H insertion via **TS-45a** leads to a platinum(IV) hydride intermediate **5a** that is endergonic by 24.5 kcal/mol and resides in a shallow well (Figure 5). The barrier for subsequent methane reductive elimination via **TS-56a** (Figure 3) is 0.4 kcal/mol (1.2 kcal/mol on the enthalpy surface) higher in free energy than the reverse barrier to give the C−H coordination complex. The B3LYP functional optimized structures also predict methane reductive elimination to be higher than the C−H bond insertion transition state by 0.4 kcal/mol on the free energy surface and 5.3 kcal/mol on the enthalpy surface. Inclusion of solvation free energy corrections (2,2,2-trifluoroethanol) increases the free energy difference to 1.5 kcal/mol. The resulting methane coordination complex, **6a** (Figure 6), has a free energy of 15.0 kcal/mol relative to **3a**. Similar to **4a**, **6a** has a structure that indicates an agostic interaction between one of the methane C−H (1.126 Å) bonds and the Pt center (Pt−H = 2.003 Å). We have also confirmed that the methane elimination transition states after insertion into a methylene C−H bond are several kcal/mol higher than the pathway shown in Figure 5.

Dissociation of methane allows for the necessary vacant coordination site, and subsequent methylene C−H bond β-hydride elimination via **TS-67a** with a free energy of 18.2 kcal/mol gives the alkene platinum hydride complex **7a** (ΔG = −2.1 kcal/mol; Figure 5). As expected, in **TS-67a** the C−H bond is stretched to 1.355 Å and the forming Pt−H (1.743 Å) bond is product-like. The forming alkene (C−C = 1.448 Å) distance is intermediate between the single and double bond length. The resulting

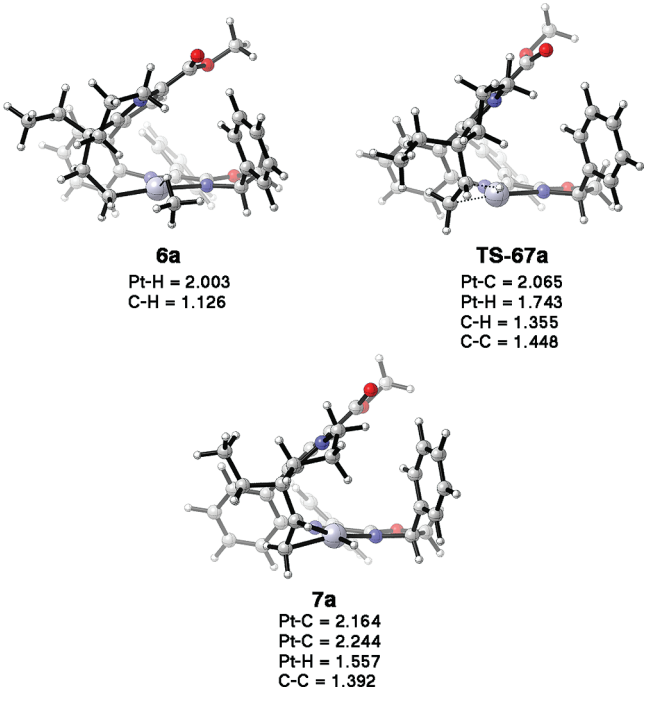

Figure 6. Methane coordination complex (**6a**), β-hydride elimination transition structure (**TS-67a**), and alkene platinum hydride (**7a**).

platinum hydride complex **7a** shows the expected four-coordinate square planar bonding arrangement. Because the alkene

dx.doi.org/10.1021/jo201234f |J. Org. Chem. 2011, 76, 7180–7185

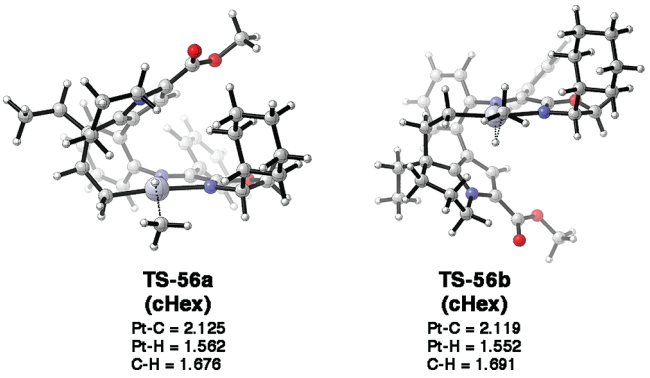

Figure 7. Methane elimination transition states with the cyclohexyl oxazolinyl ligand.

ligand coordinates in an intramoleuclar fashion the terminal alkene carbon has a much shorter Pt−C distance (2.164 Å) than the internal alkene carbon (Pt−C = 2.244 Å).

3.4. Origin of Diastereoselectivity. The asymmetric synthesis of (−)-rhazinilam was accomplished by Sames and co-workers because the chiral oxazolinyl Pt ligand distinguishes between enantiotopic ethyl groups (Scheme 2). The experimental ratio of **7a**:**7b** (and **8a**:**8b**) found using the phenyl oxazolinyl ligand at 60 °C was 6:1. As discussed in the introduction, the ratio of **3a** to **3b** is constant during thermolysis. This requires interconversion between **3a** and **3b** prior to C−H activation and functionalization. Based on the free energy surface shown in Figure 5, **TS-56a** controls the rate of forming diastereomer **7a**. A similar C−H insertion and methane reductive elimination pathway is also preferred over metathesis pathways or pathways that involve insertion into a methylene C−H bond for conversion of **3b** into **7b**. The insertion and methane elimination transition states for **3b** are shown in Figure 3 (Section 3.2). The free energy difference between **TS-45b** and **3b** is 27.0 kcal/mol. Similar to the free energy surface shown in Figure 5, C−H bond insertion is a reversible step and has a lower barrier than methane elimination. The free energy for methane elimination via **TS-56b** is 33.4 kcal/mol relative to **3b**. Because **3a** and **3b** equilibrate during the reaction the diastereoselectivity is the result of competing methane elimination transition states, **TS-56a** and **TS-56b**. The free energy difference between these transition structures is 4.7 kcal/mol. The enthalpy difference is 6.3 kcal/mol. With the 6-311+G(2d,p)/LAN2TZ(f) basis set using the 6-31G-(d,p)/LANL2DZ enthalpy and entropy corrections the free energy difference between **TS-56a** and **TS-56b** is 3.8 kcal/mol. The B3LYP optimized geometries predict a free energy difference of 0.5 kcal/mol and an enthalpy difference of 2.3 kcal/mol. In accord with experiment, M06 and B3LYP both predict that **TS-56a** is lower in energy than **TS-56b**. However, M06 significantly overestimates the selectivity while the B3LYP energy difference is (likely fortuitously) more in accord with experiment.

Comparison of the lower energy transition structure **TS-56a** versus **TS-56b** shows that the origin of selectivity is not a destabilizing steric interaction. In **TS-56a** the phenyl group is on the same face as the pyrrole ring and methyl carboxylate group. In **TS-56b** the phenyl group is on the opposite face. This indicates that the oxazolinyl ligand induces selectivity via weak stabilizing interactions between the carboxylate group and the phenyl group. The distances between the closest oxazolinyl phenyl ring hydrogen atoms and carboxylate oxygen atoms are 2.300 and 2.800 Å. These distances suggest that dispersion interactions as well as dipole−dipole interactions between the phenyl group C−H bond and carboxylate oxygen atoms are responsible for selectivity.

Change from the phenyl to a cyclohexyl oxazolinyl ligand also shows preference for **TS-56a** over **TS-56b** (Figure 7). M06 predicts a 3.9 kcal/mol free energy difference between these transition structures while B3LYP predicts a 2.8 kcal/mol free energy difference. Interestingly, M06 incorrectly predicts that the cyclohexyl oxazolinyl ligand would be slightly less selective than the phenyl oxazolinyl ligand whereas B3LYP correctly predicts an exaggerated increase in selectivity. Again, inspection of the **TS-56a** in Figure 7 shows that the cyclohexyl group is congested and on the same side as the pyrrole ring and methyl carboxylate group while in the disfavored **TS-56b** the cyclohexyl group is uncrowded. This again indicates that weak stabilizing forces rather than steric destabilizing forces give rise to stereoselectivity.

4. CONCLUSION

In conclusion, we have shown that the key C−H activation and functionalization steps in the synthesis of rhazinilam starting from **3a** proceeds via an insertion (oxidative addition) mechanism of a primary C−H bond in preference to activation of the secondary methylene C−H bond. After C−H activation, rate- and selectivity-determining methane elimination followed by β-hydride elimination gives the alkene platinum hydride complex. Diastereoselectivity was revealed to originate from stabilizing weak interactions between the phenyl (or cyclohexyl) group of the chiral oxazolinyl ligand and the carboxylate group.

■ ASSOCIATED CONTENT

Supporting Information. M06 grid comparison, CCSD(T) energy comparison, full refs 14 and 16, and *xyz* coordinates of stationary points. This material is available free of charge via the Internet at http://pubs.acs.org.

■ AUTHOR INFORMATION

Corresponding Author
*E-mail: dhe@chem.byu.edu.

■ ACKNOWLEDGMENT

We thank BYU for financial support. We also thank the Fulton Supercomputing Lab for computational support. This work was supported as part of the Center for Catalytic Hydrocarbon Functionalization, an Energy Frontier Research Center Funded by the U.S. Department of Energy, Office of Science, Office of Basic Energy Sciences, under Award Number DE-SC0001298. We also acknowledge the American Chemical Society Petroleum Research Fund for support. C.S.E. acknowledges support from a BYU chemistry department research award.

■ REFERENCES

(1) (a) Ritleng, V.; Sirlin, C.; Pfeffer, M. *Chem. Rev.* **2002**, *102*, 1731. (b) Godula, K.; Sames, D. *Science* **2006**, *312*, 67. (c) Colby, D. A.; Bergman, R. G.; Ellman, J. A. *Chem. Rev.* **2010**, *110*, 624.

(2) (a) Labinger, J. A.; Bercaw, J. E. *Nature* **2002**, *417*, 507. (b) Bergman, R. G. *Nature* **2007**, *446*, 391.

(3) For examples of possible direct C−H bond functionalization, see: (a) Hinman, A.; Du Bois, J. *J. Am. Chem. Soc.* **2003**,

125, 11510. (b) Das, S.; Incarvito, C. D.; Crabtree, R. H.; Brudvig, G. W. *Science* **2006**, *312*, 1941. (c) Chen, M. S.; White, C. S. *Science* **2007**, *318*, 783. For a review of selective C−H bond oxidation, see: (d) Newhouse, T.; Baren, P. S. *Angew. Chem., Int. Ed.* **2011**, *50*, 3362.

(4) Volume 110, Issue 2, of the journal *Chemical Reviews* provides review articles on the topic of C−H bond activation and functionalization. For example, see: (a) Crabtree, R. H. *Chem. Rev.* **2010**, *110*, 575. (b) Colby, D. A.; Bergman, R. G.; Ellman, J. A. *Chem. Rev.* **2010**, *110*, 624. For a review on computational C−H activation, see: (c) Balcells, D.; Clot, E.; Eisenstein, O. *Chem. Rev.* **2010**, *110*, 749.

(5) There are numerous examples of ligand directed C−H bond activation. For early reviews, see: (a) Ryabov, A. D. *Chem. Rev.* **1990**, *90*, 403. (b) Dyker, G. *Angew. Chem., Int. Ed* **1999**, *38*, 1690. For a recent review, see: (c) Lyons, T. W.; Sanford, M. S. *Chem. Rev.* **2010**, *110*, 1147 and references therein. (d) For a recent example, see: Wang, D.-H.; Engle, K. M.; Shi, B.-F.; Yu, J.-Q. *Science* **2010**, *327*, 315.

(6) (a) O'Malley, S. J.; Tran, K. L.; Watzke, A.; Bergman, R. G.; Ellman, J. A. *J. Am. Chem. Soc.* **2005**, *127*, 13496. (b) Wang, D.-H.; Yu, J.-Q. *J. Am. Chem. Soc.* **2011**, *133*, 5767.

(7) Tasi, A. S.; Bergman, R. G.; Ellman, J. A. *J. Am. Chem. Soc.* **2008**, *130*, 6316.

(8) (a) Johnson, J. A.; Sames, D. *J. Am. Chem. Soc.* **2000**, *122*, 6321. (b) Johnson, J. A.; Li, N.; Sames, D. *J. Am. Chem. Soc.* **2002**, *124*, 6900.

(9) For rhazinilam synthesis without C−H activation see references 9−11. (a) Bowie, A. L.; Hughes, C. C.; Trauner, D. *Org. Lett.* **2005**, *7*, 5207. (b) Bowie, A. L.; Traunder, D. *J. Org. Chem.* **2009**, *74*, 1581.

(10) Beck, E. M.; Hatley, R.; Gaunt, M. J. *Angew. Chem., Int. Ed.* **2008**, *47*, 3004.

(11) (a) Ratcliffe, A. H.; Smith, G. F.; Smith, G. N. *Tetrahedron Lett.* **1973**, *14*, 5179. (b) Magnus, P.; Rainey, T. *Tetrahedron* **2001**, *57*, 8647. (c) Liu, Z.; Wasmuth, A. S.; Nelson, S. G. *J. Am. Chem. Soc.* **2006**, *128*, 10352. (d) Gu, Z.; Zakarian, A. *Org. Lett.* **2010**, *12*, 4224.

(12) Zhao, Y.; Truhlar, D. G. *Theor. Chem. Acc.* **2008**, *120*, 215.

(13) Wheeler, S. E.; Houk, K. N. *J. Chem. Theory Comput.* **2010**, *6*, 395.

(14) Frisch, M. J.; et al. *Gaussian 09*, revision A.02; Gaussian, Inc.: Wallingford, CT, 2009.

(15) (a) Becke, A. D. *J. Chem. Phys.* **1993**, *98*, 5648. (b) Lee, C.; Yang, W.; Parr, R. G. *Phys. Rev. B* **1988**, *37*, 785. (c) Vosko, S. H.; Wilk, L.; Nusair, M. *Can. J. Phys.* **1980**, *58*, 1200.

(16) Frisch, M. J.; et al. *Gaussian 03*, revision D.01; Gaussian, Inc.: Wallingford, CT, 2004.

(17) CYLview, 1.0b; Legault, C. Y. Université de Sherbrooke, 2009 (http://www.cylview.org).

(18) Zhao, Y.; Truhlar, D. G. *Acc. Chem. Res.* **2008**, *41*, 157.

(19) (a) Sieffert, N.; Bühl, M. *Inorg. Chem.* **2009**, *48*, 4622. (b) Minenkov, Y.; Occhipinti, G.; Jensen, V. R. *J. Phys. Chem. A* **2009**, *113*, 11833. (c) Stewart, I. C.; Benitez, D.; O'leary, D. J.; Tkatchouk, E.; Day, M. W.; Goddard, W. A., III; Grubbs, R. H. *J. Am. Chem. Soc.* **2009**, *131*, 1931. (d) Benitez, D.; Tkatchouk, E.; Goddard, W. A., III. *Organometallics* **2009**, *28*, 2643. (e) Fedorov, A.; Couzijn, E. P. A.; Nagornova, N. S.; Boyarkin, O. V.; Rizzo, T. R.; Chen, P. *J. Am. Chem. Soc.* **2010**, *132*, 13789. (f) Takatani, T.; Sears, J. S.; Sherrill, C. D. *J. Phys. Chem. A* **2010**, *114*, 11714. (g) Pratt, L. M.; Voit, S.; Okeke, F. N. *J. Phys. Chem. A* **2011**, *115*, 2281. (h) Kulkarni, A. D.; Truhlar, D. G. *J. Chem. Theory Comput.* **2011**, *7*, 2325.

(20) (a) Hay, P. J.; Wadt, W. R. *J. Chem. Phys.* **1985**, *82*, 270. (b) Hay, P. J.; Wadt, W. R. *J. Chem. Phys.* **1985**, *82*, 284. (c) Hay, P. J.; Wadt, W. R. *J. Chem. Phys.* **1985**, *82*, 299. (d) Ehlers, A. W.; Bohme, M.; Dapprich, S.; Gobbi, A.; Hollwarth, A.; Jonas, V.; Kohler, K. F.; Stegmann, R.; Veldkamp, A.; Frenking, G. *Chem. Phys. Lett.* **1993**, *208*, 111. (e) Roy, L. E.; Hay, P. J.; Martin, R. L. *J. Chem. Theory Comput.* **2008**, *4*, 1029.

(21) Marenich, A. V.; Cramer, C. J.; Truhlar, D. G. *J. Phys. Chem. B* **2009**, *113*, 6378.

(22) (a) Heiberg, H.; Swang, O.; Ryan, O. B.; Gropen, O. *J. Phys. Chem. A* **1999**, *103*, 10004. (b) Heiberg, H.; Johansson, L.; Gropen, O.; Ryan, O. B.; Swang, O.; Tilset, M. *J. Am. Chem. Soc.* **2000**, *122*, 10831. (c) Gilbert, T. M; Hristov, I.; Ziegler, T. *Organometallics* **2001**, *20*, 1183. (d) Hristov, I. H.; Ziegler, T. *Organometallics* **2003**, *22*, 1668. (e) Zhu, H.; Ziegler, T. *Organometallics* **2007**, *26*, 2277. (f) Zhu, H.; Ziegler, T. *Organometallics* **2008**, *27*, 1743. (g) Zhu, H.; Ziegler, T. *Organometallics* **2009**, *28*, 2773. (h) Butschke, B.; Schröder, D.; Schwarz, H. *Organometallics* **2009**, *28*, 4340. (i) For experimental work, see the work of Labinger and Bercaw. For example: Zhong, H. A.; Labinger, J. A.; Bercaw, J. E. *J. Am. Chem. Soc.* **2002**, *124*, 1378. (j) For a review, see: Lin, Z. *Coord. Chem. Rev.* **2007**, *251*, 2280.

(23) B3LYP predicts a 12.2 and 11.0 kcal/mol free energy and enthalpy difference between the lowest energy metathesis and lowest energy insertion transition state.